Published in final edited form as:
Nat Genet. 2010 July ; 42(7): 619–625. doi:10.1038/ng.594.

Mutations in *TMEM216* perturb ciliogenesis and cause Joubert, Meckel and related syndromes

Enza Maria Valente[1,2,*], **Clare V. Logan**[3,*], **Soumaya Mougou-Zerelli**[4,5,*], **Jeong Ho Lee**[6,*], **Jennifer L. Silhavy**[6], **Francesco Brancati**[1,7], **Miriam Iannicelli**[1], **Lorena Travaglini**[1], **Sveva Romani**[1], **Barbara Illi**[1], **Matthew Adams**[3], **Katarzyna Szymanska**[3], **Annalisa Mazzotta**[1], **Ji Eun Lee**[6], **Jerlyn C. Tolentino**[6], **Dominika Swistun**[6], **Carmelo D. Salpietro**[2], **Carmelo Fede**[2], **Stacey Gabriel**[8], **Carsten Russ**[8], **Kristian Cibulskis**[8], **Carrie Sougnez**[8], **Friedhelm Hildebrandt**[9], **Edgar A. Otto**[9], **Susanne Held**[9], **Bill H. Diplas**[10], **Erica Davis**[10], **Mario Mikula**[11], **Charles M. Strom**[11], **Bruria Ben-Ze'ev**[12], **Dorit Lev**[13], **Tally Lerman Sagie**[13], **Marina Michelson**[13], **Yuval Yaron**[14], **Amanda Krause**[15], **Eugen Boltshauser**[16], **Nadia Elkhartoufi**[17], **Joelle Roume**[18], **Stavit Shalev**[19], **Arnold Munnich**[4,17], **Sophie Saunier**[20], **Chris Inglehearn**[3], **Ali Saad**[5], **Adila Alkindy**[21,#], **Sophie Thomas**[4], **Michel Vekemans**[4,17], **Bruno Dallapiccola**[22], **Nicholas Katsanis**[10], **Colin A. Johnson**[3,+], **Tania Attié-Bitach**[4,17,+], and **Joseph G. Gleeson**[6,+]

[1]Mendel Laboratory, Istituto di Ricovero e Cura a Carattere Scientifico "Casa Sollievo della Sofferenza", 71013 San Giovanni Rotondo, Italy [2]Department of Medical and Surgical Paediatric Sciences, University of Messina, Messina, Italy [3]Section of Ophthalmology and Neurosciences, Wellcome Trust Brenner Building, Leeds Institute of Molecular Medicine, St James's University Hospital, Leeds, LS9 7TF, U.K. [4]Département de Génétique, INSERM U781, Hôpital Necker-Enfants Malades, Université Paris Descartes, Paris, France [5]Service de Cytogénétique, Génétique moléculaire et Biologie de la Reproduction, Hôpital Farhat Hached, Sousse, Tunisia [6]Neurogenetics Laboratory, Institute for Genomic Medicine, Department of Neurosciences and Pediatrics, Howard Hughes Medical Institute, University of California, San Diego, 92093, USA [7]Department of Biomedical Sciences and Aging Research Center, Ce.S.I., G. d'Annunzio University Foundation, Chieti, Italy [8]Genome Sequencing and Analysis Program, Broad Institute, Cambridge, MA 02141, USA [9]Department of Pediatrics, Howard Hughes Medical Institute, University of Michigan, Ann Arbor, MI 48109-5646, USA [10]Center for Human Disease Modeling, Duke University, Durham NC 27710, USA [11]Quest Diagnostics Inc. Nichols Institute, San Juan Capistrono, CA 92690, USA [12]Safra Pediatric Hospital, Pediatric Neurology Unit, Sheba Medical

Correspondence should be addressed to J.G.G. (jogleeson@ucsd.edu), E.M.V. (e.valente@css-mendel.it), C.A.J. (c.johnson@leeds.ac.uk) or T.A-B. (tania.attie@inserm.fr).
[*]Contributed equally
[+]These authors jointly directed this work.
[#]Current address: Clinical Genetics, College of Medicine & Health Sciences, Sultan Qaboos University Hospital, Al-Khod, Muscat, Oman

AUTHOR CONTRIBUTIONS. J.L.S. performed fine mapping in *JBTS2*, cDNA sequencing, Northern analysis, and identified the *TMEM216* gene as mutated. F.B., M.I., L.T, A.M identified the mutation common to Ashkenazi patients and performed mutation analysis; S.G., C.R., K.C., C.S. performer mutation analysis of candidate genes in the *JBTS2/MKS2* locus; C.V.L., S.M.-Z., J.H.L., K.S., F.H., E.A.O., S.H. N.E., N.K., performed mutation analysis of *TMEM216* in cohorts of patients with ciliopathies; S.M.-Z and S.Sa. performer cilia analysis; S.T. performed cDNA expression and IHC; J.H.L., J.E.L., B.H.D., E.D. performed zebrafish experiments; C.V.L., J.H.L., S.R., B.I., M.A. C.A.J., did confocal microscopy and biochemical assays; E.M.V., J.C.T., D.S., C.D.S., C.F., ., B.B.-Z, D.L., T.L.S., M.Mic., Y.Y, A.K., E.B., J.R., S.S, A.S., A.A., B.D., C.A.J. recruited patients and detailed clinical information for the study; M.M., C.M.S. performed control genotyping in Ashkenazi cohorts; A.Mu., C.I., M.V., B.D. helped devise and supervise genetic analysis and contributed to the manuscript; E.M.V., C.A.J., T.A.-B., J.G.G. wrote the manuscript.

DATABASE ACCESSION NUMBERS. Full length *TMEM216* open reading frame is encoded in EST BI910875. Accession number for human TMEM216 protein sequence is NP_001167462.

COMPETING FINANCIAL INTERESTS. The authors declare that they have no competing financial interests.

Europe PMC Funders Author Manuscripts

Center, Ramat-Gan, Israel [13]Institute of Medical Genetics, Metabolic Neurogenetics Service, Wolfson Medical Center, Holon 58100 Israel [14]Prenatal Diagnosis Unit, Genetic Institute, Tel Aviv Sourasky Medical Center, Tel Aviv 64239, Israel [15]Division of Human Genetics, National Health Laboratory Service, School of Pathology, University of the Witwatersrand, Johannesburg 2000, South Africa [16]Department of Paediatric Neurology, University Children's Hospital of Zurich, CH-8032, Zurich, Switzerland [17]Département de Génétique, Hôpital Necker-Enfants Malades, Assistance Publique Hôpitaux de Paris (APHP), France [18]Génétique Médicale, CHI Poissy, Saint Germain en Laye, France [19]The Genetics Institute, Ha'Emek Medical Center, Afula, Israel [20]INSERM U983, Hôpital Necker-Enfants Malades, Université Paris Descartes, Hôpital Necker-Enfants Malades, APHP, Paris, France [21]University Hospital of Wales, Heath Park, Cardiff, CF14 4XW, U.K. [22]Istituto di Ricovero e Cura a Carattere Scientifico "Bambino Gesù Hospital", Rome, Italy

Abstract

Joubert syndrome (JBTS), related disorders (JSRD) and Meckel syndrome (MKS) are ciliopathies. We now report that *MKS2* and *JBTS2* loci are allelic and due to mutations in *TMEM216*, encoding an uncharacterized tetraspan transmembrane protein. *JBTS2* patients displayed frequent nephronophthisis and polydactytly, and two cases conformed to the Oro-Facio-Digital type VI phenotype, whereas skeletal dysplasia was common in MKS fetuses. A single p.R73L mutation was identified in all patients of Ashkenazi Jewish descent (n=10). TMEM216 localized to the base of primary cilia, and loss of TMEM216 in patient fibroblasts or following siRNA knockdown caused defective ciliogenesis and centrosomal docking, with concomitant hyperactivation of RhoA and Dishevelled. TMEM216 complexed with Meckelin, encoded by a gene also mutated in JSRD and MKS. Abrogation of *tmem216* expression in zebrafish led to gastrulation defects that overlap with other ciliary morphants. The data implicate a new family of proteins in the ciliopathies, and further support allelism between ciliopathy disorders.

The neurological features of JSRD include hypotonia, ataxia, psychomotor delay, irregular breathing pattern and oculomotor apraxia and are variably associated with multiorgan involvement, mainly retinal dystrophy, nephronophthisis (NPH) and congenital liver fibrosis. JSRD are genetically heterogeneous, and all known genes encode proteins localized at or near the primary cilium1. We previously mapped the *JBTS2* (also known as *CORS2*) locus to chromosome 11p12-q13.3 in a large Sicilian family and in three consanguineous pedigrees from the Middle East2-3. Aligning the two datasets suggested a minimal candidate interval between D11S1344 and D11S1883 (46.123-63.130 Mb)4 (Fig. 1a**)**.

Overlapping with JSRD is MKS, characterized by occipital encephalocele and other posterior fossa defects, cystic dysplastic kidneys, hepatic bile duct proliferation and polydactyly, and the two conditions are known to be allelic at four loci5-8. The *MKS2* locus was initially mapped in families of North African and Middle Eastern ancestry to a chromosome 11q region telomeric to *JBTS29*, but our subsequent identification of additional families, as well as SNP re-analysis of the initial family, indicated allelism with *JBTS2* between rs1113480 and rs953894 (48.014-62.518 Mb) (Supplementary Fig. 1). Because JSRD and MKS are considered ciliopathies, of the 200 total candidate genes, we first sequenced the exons and splice sites of genes listed in the cilia proteome databases10-11 in one affected subject from each *JBTS2/MKS2* family, but no mutations were identified.

Tetraspan transmembrane proteins are characterized by four hydrophobic, putative transmembrane domains (TM1-TM4), forming two extracellular and one intracellular loop,

which regulate signaling and trafficking properties of their partner proteins in multiple cellular contexts12. While little is known about their function, they can act with Wnt receptors13, and their ability to form complexes with a wide variety of membrane and cytosolic proteins14 suggests that they may participate in the formation of membrane domains that regulate signaling and sorting processes. Transmembrane proteins also represented attractive candidates, due to similarities to *MKS3/TMEM67* encoding Meckelin, which is mutated both in JSRD and MKS5,15. Therefore we additionally sequenced the eight genes encoding transmembrane proteins, eventually identifying homozygous deleterious mutations in *TMEM216* in six of the 12 JSRD/MKS families compatible with linkage to the locus (Table 1). Interestingly, residue p.R73 was mutated both in a Sicilian family with JSRD (COR000, p.R73L) and in a Turkish family, in which MKS and JSRD coexisted in the same sibship (COR114/F37, p.R73H). The p.G77A mutation in two Palestinian families (F56, F58) resulted from a substitution (c.230G>C) that affects the first base of exon 5, leading to the use of an alternative splice site in intron 4, the inclusion of an additional 46bp and resultant premature protein termination (p.T78KfsX30) (Supplementary Fig. 2**)**. None of these mutations were identified in over 500 controls from ethnically matched cohorts.

We next screened an additional 460 JSRD and 132 MKS probands (**Supplementary Note**) and identified mutations in 12 and two further cases, respectively (Table 1). Twelve of 14 JSRD families shared the same homozygous p.R73L founder mutation, including two families from Sicily and ten families of Ashkenazi Jewish descent. Saturation of the region surrounding the p.R73L mutation with 17 SNP/microsatellite markers indicated that these families shared the same ancestral haplotype, spanning 472 Kb around the mutation (Supplementary Fig. 3**)**, that could be dated back at least 20 generations. The carrier frequency in the Ashkenazi population was determined to be about 1:100, as we identified two heterozygous healthy unrelated carrier individuals among a screened cohort of 212 Ashkenazi individuals, making carrier detection possible at least in this population. A similar carrier frequency of 1:92 has also been determined for the p.R73L mutation in a distinct study on eight Ashkenazi *JBTS2* families and 2766 unaffected controls16. Microsatellite analysis also detected shared haplotypes in the two Palestinian (F56, F58) and in the two Tunisian families (F2, F5), homozygous for the same mutations (Supplementary Fig. 1).

Overall, 20 JSRD patients and 11 MKS fetuses carried *TMEM216* mutations (Fig. 1b**,** Table 1). All of the nonsynonymous changes occurred in evolutionarily conserved residues (Fig. 1c-d), and led to unstable protein when transfected into heterologous cells (Fig. 1e**,** Supplementary Fig. 4). Although truncating mutations were identified in both the middle and end of the protein, p.R73 transversions predominated (Fig. 1c), with the p.R73L clearly a founder mutation. Among JSRD, the phenotype was characterized by frequent occurrence of NPH (9/20) and polydactyly (9/20), while retinal dystrophy and congenital hepatic fibrosis were never observed. In keeping with this, sequence analysis of 96 patients with Bardet-Biedl syndrome identified no homozygous mutations, since retinopathy is a key feature of this condition. In two JSRD patients (MTI161 and MTI467), polydactyly was associated with either tongue tumors or multiple oral frenula, corresponding to the Oro-Facio-Digital type VI (or Varadi-Papp) syndrome16 (OMIM%277170), indicating that *TMEM216* mutations are the first known identified cause. In the 11 MKS fetuses with *TMEM216* mutations, distinctive clinical features were skeletal dysplasia, including intrauterine growth retardation or bowing of the long bones in six fetuses, cleft palate in four, and anencephaly in two (Table 1**,** Supplementary Fig. 5).

TMEM216 is a poorly annotated gene, with RefSeq predicting a protein of just 86 aa, suggesting potential alternative splicing. To characterize this mRNA we performed Northern

analysis with a commercial human fetal blot, and found a single major mature isoform at about 1.4 Kb (Supplementary Fig. 6a), agreeing with the predicted 1.3 Kb of the longest representative cDNAs. To interrogate splicing we designed primers complementary to the furthest 5′ and 3′ regions of the known cDNA, and sequenced 48 cloned PCR products from a 20 week gestation human fetal brain library. We identified four major splice isoforms, the longest and most prevalent predicting a protein of 148 aa (Supplementary Fig. 6b), which we consider to be the full-length mRNA. There is also extensive alternative splicing, encoding very short proteins (Supplementary Fig. 6b), the functions of which were not evaluated further. Importantly, we did not find any mutations in any of the putative UTRs.

To elucidate roles for *TMEM216* in human development, we first examined its expression in human embryonic tissues. *In situ* hybridization analysis in human embryos confirmed expression in the central nervous system, limb bud, kidney and cartilage (Supplementary Fig. 6c-h), which is similar to the broad and relatively low-level expression pattern of other JSRD/MKS genes. We next raised an anti-TMEM216 polyclonal affinity-purified antibody against aa 81-90, demonstrated specificity (Supplementary Fig. 7a-b), and immunostained two different ciliated cell lines (inner medullary collecting duct [IMCD3] and retinal pigment epithelium [hRPE]). We observed localization with the base of the primary cilium or adjacent basal body in the majority of cells, as marked by either acetylated or glutamylated tubulin staining (Fig. 2a-d). TMEM216 antibody also reacted strongly to the base of cilia in organs like kidney containing ciliated cells (Fig. 2c**,** Supplementary Fig. 7c), but failed to react with these structures in hTERT-immortalized fetal *TMEM216* p.R85X homozygous mutant fibroblasts (Supplementary Fig. 7d**)**. Epitope-tagged TMEM216 showed similar localization to the base of cilia and other microtubule structures (i.e. mitotic spindle in cells undergoing late telophase, Supplementary Fig. 8).

In *TMEM216* p.R85X mutant fibroblasts, we noticed a failure in ciliogenesis following 48 hr serum starvation (Fig. 3a) compared with controls. Western analysis of whole cell lysates from control fibroblasts identified a band at 19 kD (Fig. 3b), matching the predicted 148 aa full length protein, whereas this band was attenuated or lost in *TMEM216* p.R85X fibroblasts or in IMCD3 cells in which *Tmem216* was knockded down.

To determine the basis of the ciliogenesis defect, we performed transient transfection of monolayers of IMCD3 cells with two separate *Tmem216* siRNA duplexes. *Tmem216* knockdown prevented ciliogenesis in polarized cells, and blocked correct docking of centrosomes at the apical cell surface (Fig. 3c), as seen previously for Meckelin and MKS117. This ciliogenesis defect was quantified by comparing the percentage of cells with cilia (defined as > 1 μm length) vs. those without cilia (< 1μm length), and by analyzing the percentage of cells with centrosomes located apical to the nucleus. In cells in which *Tmem216* was knocked down, we observed a striking defect in both of these measurements compared with two separate control transfections (Fig. 3d-e**,** chi-squared test, $p<0.001$, for 350 cells from each condition), suggesting its requirement in centrosome docking.

The similarities in cellular phenotypes of *Mks3* and *Tmem216* knockdown, and subcellular localizations of Meckelin and TMEM216, prompted us to ask if the two proteins could interact. Firstly, GFP-tagged TMEM216 was immunoprecipitated with antibodies to either N- or C-terminal portions of Meckelin (Fig. 4a) and, secondly, the reciprocal IP experiment used α-GFP antibody to pull down Meckelin (Fig. 4b). Both assays detected a complex between TMEM216 and Meckelin.

Many aspects of actin-dependent polarized cell behavior, including morphogenetic cell movements18 and ciliogenesis19, are mediated by the planar cell polarity (PCP) pathway of

non-canonical Wnt signaling20. We therefore first examined RhoA, since the Rho family of small GTPases are key mediators of this pathway20-21. Consistent with previous results following *MKS3* loss22, we found that RhoA signaling was hyperactived in both *TMEM216* p.R85X fibroblasts or following *Tmem216* knockdown (Fig. 4c-d), despite normal total amounts of RhoA in these cells. Centrosome docking at the apical cell surface is prevented by the interruption of actin remodeling23, and is dependent on both RhoA activation and regulation by the core PCP protein Dishevelled (Dvl)24. We confirmed that RhoA is localized to the basal body in confluent IMCD3 cells but, following *Tmem216* knockdown for 24 hr, RhoA was mislocalized to peripheral regions of the basal body and to basolateral cell-cell contacts (Fig. 4e), consistent with translocation of ectopically-activated RhoA to the cytosol25. *Tmem216* knockdown also showed evidence of a mislocalization of γ-tubulin at the centrosome/basal body for this timepoint, which suggests a defect in γ-tubulin nucleation, one of the earliest steps in ciliogenesis26. The established role of RhoA in modulating the actin cytoskeleton in the PCP pathway then led us to evaluate *MKS2* patient fibroblast lines for alterations. We found a co-localization of actin stress fibers and the actin cross-linker filamin-A in the cytoplasm of these mutant cells, which was absent in control (Fig. 4f).

We next looked at Dvl signaling in cells, since cilia negatively regulate Dvl activation27, and Dvl mediates Rho activation at the apical surface of ciliated epithelial cells24. We found that loss of TMEM216 increased phosphorylation of Dvl1 (Fig. 5a **left and right panel**), implying that TMEM216 modulates hyper-responsiveness of signaling pathways mediated by Dvl and RhoA. We found that Rho inhibition also increased the Dvl1 phosphorylation in ciliated cells, supporting the existence of feedback mechanism between Rho and Dvl (Fig. 5a**, right panel)**. Unexpectedly, the constitutive Dvl1 phosphorylation associated with TMEM216 loss was blocked by Rho inhibition (Fig. 5a**, right panel**), suggesting that this loss in ciliated cells can modify the feedback mechanism. Although this possibility warrants further investigation, our data nevertheless suggest a working model in which Dvl1, RhoA and TMEM216 may serve as part of a complex in the pericentrosomal compartment to mediate cellular polarization and centrosomal apical docking. Previous studies have shown that Dvl and Rho contribute to a core framework for regulating the apical docking of centrosomes24, and we also see evidence of a common complex containing TMEM216, Dvl1 and RhoA in TMEM216-transfected cells (Fig. 5b). Since we saw no difference in the localization of Dvl1 following *Tmem216* knockdown **(**Supplementary Fig. 9), these data predict that the hyperactivation of Rho in the absence of TMEM216 might be responsible for the centrosome docking defect at the apical cellular surface. As expected, we found that the impaired centrosome docking caused by *Tmem216* knockdown was rescued in a dose-dependent fashion using Rho inhibitor (Fig. 5c).

Meckelin is proposed to regulate centrosomal docking through the RhoA signaling pathway22, and bears similarity to the Frizzled family of transmembrane Wnt receptors15. Direct evidence of a role for Meckelin in PCP signaling stems from zebrafish embryo morphant phenotypes following morpholino knock-down of *mks328*. These included defects in gastrulation movement (a shortened body axis, broad notochords and misshapen somites), which are typical of defects in non-canonical (PCP) Wnt signaling, and have been observed in numerous ciliary and basal body morphants28-29. We observed identical ciliary phenotypes in *tmem216* morphants, which were largely rescued by RNA encoding human *TMEM216* (Fig. 5d), and fully rescued by RNA encoding non-targetable zebrafish *tmem216* (not shown). We therefore directly compared the *tmem216* and *mks3* morphant phenotypes in zebrafish, and noted similar defects in both live embryos and in embryros in which pronephric mesoderm, anterior neural structures, adaxial mesodermal cells, and somites were labeled with a *krox20, pax2*, and *myoD* riboprobe cocktail (Fig. 5e-f). Quantification demonstrated alteration of convergence to the midline and extension along the AP axis

consistent with a PCP defect, although the AP extension defect was more pronounced in the *mks3* compared to the *tmem216* morphant.

Recent work has implicated the tetraspanin TSPAN12 in the regulation of Norrin signaling by the Wnt receptor Frizzled-4 and coreceptor LRP513. We therefore speculate that TMEM216, a novel tetraspan protein, forms a non-canonical Wnt receptor-coreceptor complex with Meckelin. Our data support a role for both proteins in mediating PCP signaling through the RhoA pathway to cause actin cytoskeleton rearrangements, although whether Rho functions upstream or downstream of Dvl1 remains to be determined. In apical regions of the cell, such actin reorganization would be an essential step before the centrosome/basal body could dock correctly and initiate ciliogenesis. The identification of mutations in *TMEM216* as a cause of JSRD and MKS therefore further emphasizes the interrelationship between cell polarity, cellular morphogenesis and signal transduction pathways.

Supplementary Material

Refer to Web version on PubMed Central for supplementary material.

Acknowledgments

We thank Marshfield Clinic Research Foundation, Center for Inherited Disease Research (supported by the NIH NHBLI) for genotyping support, Adam Felsenfeld and the Medical Sequencing Initiative at NHGRI, and support for sequencing from the Broad Institute and the Broad Sequencing Platform, Jennifer Meerloo at the UCSD Neurosciences Microscopy Core (Supported by NINDS P30NS047101). We thank Chaim Jalas at Bonei Olam Center for Rare Jewish Genetic Disorders, Brooklyn, NY, Michael R. Eccles at University of Otago, Dunedin, New Zealand, Heather M. Harville at University of Michigan, Gaetano Tortorella, Silvana Briuglia, Roberto Chimenz, Romina Gallizzi and Marilena Briguglio at University of Messina, Italy, and the SOFFOET (French SOciety of FOETalpathology) for patient referrals. We thank Ewan Morrison, Peter Novick and Susan Ferro-Novick for helpful discussions and Dr. Carsten Janke for GT335 antibody. We thank Emmanuel Genin for linkage analysis, Sophie Audolent, Candice Babarit, Flora Legendre, and Helory-Mael Gaudé for technical help, and Olivier Duc for confocal microscopy. S.M-Z. is supported by INSERM-DGRSRT (CS/RN/2008 n°87), and N.K. is the Brumley Professor. This work was supported by the Italian Ministry of Health (RC2010, Ricerca Finalizzata 2006), Telethon Foundation Italy (GGP08145 to E.M.V.), Pierfranco and Luisa Mariani Foundation (E.M.V.), American Heart Association (J.-E.L.), BDF Newlife, the Medical Research Council (G0700073) and the Sir Jules Thorn Charitable Trust (09/JTA C.A.J.), l'Agence National pour la Recherche (ANR 07-MRAR-Fetalciliopathies T.A-B.), National Institutes of Health (R01 DK068306 F.H., R01 DK072301 R01 HD04260, R01 DK075972 N.K., NRSA fellowship F32 DK079541 E.D.D., R01 NS052455 and R01 NS04843 J.G.G., and Burroughs Wellcome Fund, and Howard Hughes Medical Institute (F.H. and J.G.G.).

Appendix

ONLINE METHODS

Research subjects

We used standard methods to isolate genomic DNA from peripheral blood of the affected children and family members or from frozen fetal tissue or amniocytes. Chromosome analysis was performed for at least one patient of each family. Informed consent was obtained from all participating families and the studies were approved by the Ethics Boards of Leeds (East), Casa Sollievo della Sofferenza, Hôpital Necker-Enfants Malades, and UCSD.

Genetic mapping

To refine the *MKS2/JBTS2* locus, the 10K Affymetrix SNP array was used to perform a genome-wide linkage search in nine consanguineous families with MKS. We performed multipoint linkage analysis using MERLIN software, assuming a fully penetrant recessive

model, a disease allele frequency of 0.001, and allowed for heterogeneity between families. Areas of homozygosity on chromosome 11 were confirmed by performing high-resolution haplotype analysis.

Mutation screening

Mutational screening of *TMEM216* was performed by direct sequencing of PCR products of the six coding exons and the adjacent intronic junctions in JSRD/MKS families showing potential linkage to the locus and all MKS cases. To test for *TMEM216* mutations in the cohort of 460 JSRD patients we applied the high resolution melting (HRM) technique30 using a LightCycler 480 (Roche Applied Science), with the same primers and optimized PCR conditions (Supplementary Table 1). Segregation of the identified mutations was investigated in all available family members. Missense mutations were excluded in the following ethnically matched controls: wildtype at p.R73 for 227 Italian and 109 Turkish; and wildtype at p.G77 and p.L114 for 158 Palestinian and 112 Tunisian individuals. All mutations were also excluded in 200 Central Asian (predominantly Pakistani), 200 European (predominantly British), as well as a cohort of 96 ethnically diverse individuals.

Founder haplotype analysis

The region surrounding *TMEM216* was saturated with 14 single nucleotide polymorphisms and three microsatellite markers in ten patients homozygous for the same p.R73L mutation. Estimation of the mutation age was calculated as reported31.

Bioinformatics

Genetic location is based on Human Genome Browser build 36.3 (http://www.genome.ucsc.edu). The ciliary proteome was searched using web-based tools10-11. RefSeq and Pfam were respectively accessed at (http://www.ncbi.nlm.nih.gov/RefSeq/) and (http://pfam.sanger.ac.uk/).

Cloning

Full-length *TMEM216* was cloned into the pcDNA3.0 vector, and then shuttled into the mCherry-, EGFP-, and FLAG- containing vectors. Mutations were introduced into TMEM216-pEGFP-N3 by QuickChange mutagenesis (Stratagene). *TMEM216* open reading frame was also cloned into pCS2+ vector in order to make RNA for injection into zebrafish embryos.

Cells and antibodies

Mouse inner medullary collecting duct (IMCD3), human hTERT-immortalized retinal pigmentary epithelial (hRPE), and human embryonic kidney (HEK293) cells were grown in Dulbecco's minimum essential medium (DMEM)/Ham's F12 supplemented with 10% fetal calf serum at 37°C/5% CO_2. Fibroblasts were immortalized with the hTERT system, and maintained in Fibroblast Growth Medium (Genlantis) supplemented with 10% fetal calf serum and 0.2 mg/ml geneticin. Normal, undiseased control fibroblasts were gestationally-age matched to fibroblasts from MKS patients22. Primary antibodies used were: mouse α-EGFP antibody (Covance MMS-118R); mouse anti-GFP and rabbit A.V. peptide ("Living Colors", Clontech); mouse anti-α-tubulin, mouse anti-γ-tubulin, mouse anti-acetylated-tubulin (Sigma-Aldrich); mouse-anti-glutamylated tubulin (GT335)32, rabbit-anti-γ-tubulin, rabbit-anti-Meckelin, mouse anti-β actin (Abcam); mouse anti-filamin A (AbNova); and mouse anti-Dvl1 (Santa Cruz Biotechnology SC-8025); mouse anti-RhoA (Cytoskeleton). Rabbit-anti-Meckelin C-terminus, raised against amino acids 982-995, has been described previously17. Rabbit-anti-Meckelin N-terminus, raised against amino acids 100-113, has also been described22. Secondary antibodies were Alexa-Fluor 488-Alexa-Fluor 594- and

Alexa-Fluor 568-conjugated goat anti-mouse IgG and goat anti-rabbit IgG (Molecular Probes), and HRP-conjugated goat anti-mouse and goat anti-rabbit (Dako). Alexa-Fluor 488 and 633 phalloidin conjugate (Molecular Probes) was used to visualize F-actin.

Biochemical assays

Constructs encoding wildtype or mutant TMEM216 were transfected into 293T cells in a ratio of 20:1 TMEM216:TK-βgal vector. Cells were lysed after 48h and samples analyzed by Western blot with α-EGFP antibody (1:500) and β-gal assay to standardize transfection efficiency33. Normalized loading levels were confirmed by blotting with α-tubulin (1:2000).

Rabbit-anti-TMEM216 antiserum was raised against the peptide sequence NLCQRKMPLS(C), comprising amino acids 81-90, by GenScript (Piscataway, NJ, USA). Antiserum was affinity-purified, and co-immunoprecipitation was performed as described previously34. Whole cell extracts (WCE) were prepared from confluent untransfected HEK293 cells, or IMCD3 cells that had been transiently transfected with 1.0 μg plasmid constructs in 90mm tissue culture dishes, or scaled down as appropriate. WCE supernatants were processed for immunoprecipitation experiments by using 5 μg affinity-purified mouse anti-GFP, or 5 μg MAbs, or 5-10 μg purified IgG fractions from rabbit polyclonal antisera, coupled to protein G- and/or protein A-sepharose beads (GE Healthcare) Immunoprecipitations were performed in reduced salt incubation buffer (20 mM Tris, pH7.5, 25 mM NaCl, 2 mM EDTA, 0.5 mM EGTA, 0.02% [w/v] NaN3, 10% [v/v] glycerol, 10% [v/v] ethanol, 0.1% [v/v] protease inhibitor cocktail). For assessing Dvl1 phosphorylation status, extraction and wash buffers were supplemented with phosphatase inhibitor cocktail (Sigma Aldrich).

In situ hybridization in human embryos

Human embryos were collected from terminated pregnancies using the mefiprestone protocol in agreement with French bioethics laws (94-654 and 04-800). Embryos were fixed in 11% formaldehyde, 60% ethanol and 10% acetic acid, embedded in paraffin and sectioned at 5 μm. Primers (Supplementary Table 1) were selected for RT-PCR amplification on RNA extracted from a whole C12 (4w) embryo to be used as template for generating the riboprobes, as described previously35. Sections were hybridized with a Digoxygenin labeled probe at 70°C overnight, and digoxygenin was detected with an anti-DIG-Fab' antibody (Roche) at 1:1000.

Immunofluorescence and confocal microscopy

IMCD3 or hTERT-immortalized fetal fibroblasts were seeded at 20×10^3 cells/well on glass coverslips in six-well plates and fixed in ice-cold methanol (5 minutes at 4°C) or 2% paraformaldehyde (20 minutes at room-temp) as described previously17,22. Confocal images were obtained using a Nikon Eclipse TE2000-E system, controlled by EZ-C1 3.50 (Nikon) software. Images were processed in Metamorph, and figures were assembled using Adobe Photoshop CS3.

Transfection and siRNA

For transfection with plasmids, cells at 90% confluency were transfected using Lipofectamine 2000 (Invitrogen). Cells were incubated for 24 to 72 hrs prior to lysis or immunostaining. For RNAi knockdown in IMCD3 cells, siRNA duplexes (Supplementary Table 1) were designed against different regions of the mouse *Tmem216* ("Stealth Select", Invitrogen). *Mks3* siRNA reagents have been described previously22. The medium or low GC non-targeting negative controls (Invitrogen) were used as scrambled siRNA controls.

Irrelevant siRNA duplexes against *Hhari* were used as a second negative control (a gift from P. Robinson, University of Leeds, UK). Individual duplexes (20 nM) or siRNA pools (total 60 nM) were transfected into IMCD3 cells at 60-80% confluency using Lipofectamine 2000 RNAiMAX (Invitrogen). The efficiency of siRNA transfections, as determined with BLOCK-iT Fluorescent Oligo (Invitrogen), was >60%. Further assays were carried out at 72 hours after transfection.

Gene expression analyses with quantitative real-time PCR

For the relative quantitation of gene expression we used quantitative real-time PCR for the standard curve method. Total RNA (1 μg) was reverse-transcribed using the Superscript III first strand cDNA system (Applied Biosystems). PCR analysis of cDNA was performed using dHPLC-purified primers (Supplementary Table 1) specific for mouse Tmem216 (Invitrogen), following optimization to eliminate primer-dimers and subsequent confirmation by analysis of amplimer dissociation curves following a qPCR run. Each reaction was run in triplicate. Amplimer levels were quantified continuously with the SYBR GreenER qPCR system (Invitrogen) using an ABI 7500 instrument, essentially as described previously15. *Hprt* RNA was amplified for normalization, quantified in Supplementary Figure 10.

RhoA activation assay

The activated GTP-bound isoform of RhoA was specifically assayed in pull-down assays using a GST fusion protein of the Rho effector rhotekin (Cytoskeleton), using conditions recommended by the manufacturers. Rho activity was inhibited by treating cells with cell permeable exoenzyme-C3-transferase (Cytoskeleton) at 2 μg/ml for 5 hr under standard cell culture conditions. Results shown are representative of three separate experiments. Full scans of all Western blots are shown in Supplementary Figure 11.

Identification of ciliary defect phenotypes in Zebrafish

To knockdown *tmem*216 in zebrafish, a translational blocking morpholino antisense oligonucleotide (MO) or control (Gene Tools) or control was microinjected (4ng/nl) into one-two cell stage embryos, obtained from natural spawning of wild-type (AB) zebrafish lines. The mRNA encoding full-length human *TMEM216* was co-injected where indicated. Endogenous *mks3* was suppressed with a splice-blocking MO described previously (3 ng/nl)28. For assessment of gastrulation phenotypes (shortened body axis, wide undulating notochord, thin and elongated somites, and small anterior structures), mid-somitic embryos were scored blind at 8 somites (live; 80-100 embryos/injection), or 10-11 somites (morphometric analyses). Embryos were fixed overnight in 4% PFA, hybridized *in situ* with DIG-labeled *krox20, pax2*, and *myoD* riboprobes according to standard protocols, and flat-mounted for imaging and analysis. At 3 days postfertilization, morphological phenotype of morphants were quantified under bright-field microscopy based upon ciliary defects (hydrocephalus, small brain, heart edema, and curved tail) or embryonic lethal phenotypes.

REFERENCES

1. Lancaster MA, Gleeson JG. The primary cilium as a cellular signaling center: lessons from disease. Curr Opin Genet Dev. 2009; 19:220–9. [PubMed: 19477114]
2. Keeler LC, et al. Linkage analysis in families with Joubert syndrome plus oculo-renal involvement identifies the CORS2 locus on chromosome 11p12-q13.3. Am J Hum Genet. 2003; 73:656–62. [PubMed: 12917796]
3. Valente EM, et al. Description, nomenclature, and mapping of a novel cerebello-renal syndrome with the molar tooth malformation. Am J Hum Genet. 2003; 73:663–70. [PubMed: 12908130]

4. Valente EM, et al. Distinguishing the four genetic causes of Joubert syndrome-related disorders. Ann Neurol. 2005; 57:513–9. [PubMed: 15786477]
5. Baala L, et al. The Meckel-Gruber syndrome gene, MKS3, is mutated in Joubert syndrome. Am J Hum Genet. 2007; 80:186–94. [PubMed: 17160906]
6. Baala L, et al. Pleiotropic Effects of CEP290 (NPHP6) Mutations Extend to Meckel Syndrome. Am J Hum Genet. 2007; 81:170–9. [PubMed: 17564974]
7. Delous M, et al. The ciliary gene RPGRIP1L is mutated in cerebello-oculo-renal syndrome (Joubert syndrome type B) and Meckel syndrome. Nat Genet. 2007; 39:875–81. [PubMed: 17558409]
8. Mougou-Zerelli S, et al. CC2D2A mutations in Meckel and Joubert syndromes indicate a genotype-phenotype correlation. Hum Mutat. 2009; 30:1574–82. [PubMed: 19777577]
9. Roume J, et al. A gene for Meckel syndrome maps to chromosome 11q13. Am J Hum Genet. 1998; 63:1095–101. [PubMed: 9758620]
10. Gherman A, Davis EE, Katsanis N. The ciliary proteome database: an integrated community resource for the genetic and functional dissection of cilia. Nat Genet. 2006; 38:961–2. [PubMed: 16940995]
11. Inglis PN, Boroevich KA, Leroux MR. Piecing together a ciliome. Trends Genet. 2006; 22:491–500. [PubMed: 16860433]
12. Hubner K, Windoffer R, Hutter H, Leube RE. Tetraspan vesicle membrane proteins: synthesis, subcellular localization, and functional properties. Int Rev Cytol. 2002; 214:103–59. [PubMed: 11893164]
13. Junge HJ, et al. TSPAN12 regulates retinal vascular development by promoting Norrin- but not Wnt-induced FZD4/beta-catenin signaling. Cell. 2009; 139:299–311. [PubMed: 19837033]
14. Caplan MJ, Kamsteeg EJ, Duffield A. Tetraspan proteins: regulators of renal structure and function. Curr Opin Nephrol Hypertens. 2007; 16:353–8. [PubMed: 17565278]
15. Smith UM, et al. The transmembrane protein meckelin (MKS3) is mutated in Meckel-Gruber syndrome and the wpk rat. Nat Genet. 2006; 38:191–6. [PubMed: 16415887]
16. Váradi V, Szabo L, Papp Z. Syndrome of polydactyly, cleft lip/palate or lingual lump, and psychomotor retardation in endogamic gypsies. J Med Genet. 1980; 17:119–22. [PubMed: 7381865]
17. Dawe HR, et al. The Meckel-Gruber Syndrome proteins MKS1 and meckelin interact and are required for primary cilium formation. Hum Mol Genet. 2007; 16:173–86. [PubMed: 17185389]
18. Wallingford JB, et al. Dishevelled controls cell polarity during Xenopus gastrulation. Nature. 2000; 405:81–5. [PubMed: 10811222]
19. Park TJ, Haigo SL, Wallingford JB. Ciliogenesis defects in embryos lacking inturned or fuzzy function are associated with failure of planar cell polarity and Hedgehog signaling. Nat Genet. 2006; 38:303–11. [PubMed: 16493421]
20. Veeman MT, Axelrod JD, Moon RT. A second canon. Functions and mechanisms of beta-catenin-independent Wnt signaling. Dev Cell. 2003; 5:367–77. [PubMed: 12967557]
21. Winter CG, et al. Drosophila Rho-associated kinase (Drok) links Frizzled-mediated planar cell polarity signaling to the actin cytoskeleton. Cell. 2001; 105:81–91. [PubMed: 11301004]
22. Dawe HR, et al. Nesprin-2 interacts with meckelin and mediates ciliogenesis via remodelling of the actin cytoskeleton. J Cell Sci. 2009; 122:2716–26. [PubMed: 19596800]
23. Pan J, You Y, Huang T, Brody SL. RhoA-mediated apical actin enrichment is required for ciliogenesis and promoted by Foxj1. J Cell Sci. 2007; 120:1868–76. [PubMed: 17488776]
24. Park TJ, Mitchell BJ, Abitua PB, Kintner C, Wallingford JB. Dishevelled controls apical docking and planar polarization of basal bodies in ciliated epithelial cells. Nat Genet. 2008; 40:871–9. [PubMed: 18552847]
25. Lang P, et al. Protein kinase A phosphorylation of RhoA mediates the morphological and functional effects of cyclic AMP in cytotoxic lymphocytes. EMBO J. 1996; 15:510–9. [PubMed: 8599934]
26. Dutcher SK. Elucidation of basal body and centriole functions in Chlamydomonas reinhardtii. Traffic. 2003; 4:443–51. [PubMed: 12795689]

27. Corbit KC, et al. Kif3a constrains beta-catenin-dependent Wnt signalling through dual ciliary and non-ciliary mechanisms. Nat Cell Biol. 2008; 10:70–6. [PubMed: 18084282]
28. Leitch CC, et al. Hypomorphic mutations in syndromic encephalocele genes are associated with Bardet-Biedl syndrome. Nat Genet. 2008; 40:443–8. [PubMed: 18327255]
29. Badano JL, et al. Dissection of epistasis in oligogenic Bardet-Biedl syndrome. Nature. 2006; 439:326–30. [PubMed: 16327777]
30. Wittwer CT. High-resolution DNA melting analysis: advancements and limitations. Hum Mutat. 2009; 30:857–9. [PubMed: 19479960]
31. Budde BS, et al. tRNA splicing endonuclease mutations cause pontocerebellar hypoplasia. Nat Genet. 2008; 40:1113–8. [PubMed: 18711368]
32. Wolff A, et al. Distribution of glutamylated alpha and beta-tubulin in mouse tissues using a specific monoclonal antibody, GT335. Eur J Cell Biol. 1992; 59:425–32. [PubMed: 1493808]
33. Lancaster MA, et al. Impaired Wnt-beta-catenin signaling disrupts adult renal homeostasis and leads to cystic kidney ciliopathy. Nat Med. 2009; 15:1046–54. [PubMed: 19718039]
34. Johnson CA, Padget K, Austin CA, Turner BM. Deacetylase activity associates with topoisomerase II and is necessary for etoposide-induced apoptosis. J Biol Chem. 2001; 276:4539–42. [PubMed: 11136718]
35. Trueba SS, et al. PAX8, TITF1, and FOXE1 gene expression patterns during human development: new insights into human thyroid development and thyroid dysgenesis-associated malformations. J Clin Endocrinol Metab. 2005; 90:455–62. [PubMed: 15494458]

Europe PMC Funders Author Manuscripts

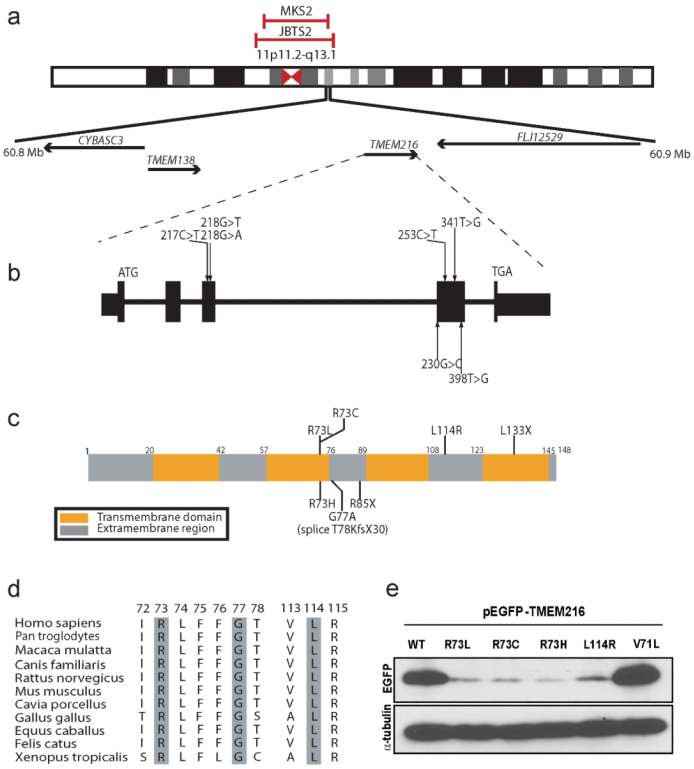

Figure 1.

Mutations in the *TMEM216* gene in patients linked to the *JBTS2* and *MKS2* loci. **(a)** Chromosomal location of the *JBTS2* and *MKS2* loci on Chr. 11cent. (**b**) *TMEM216* genomic organization, depicting start and stop codon, and location of identified base changes. **(c)** The longest splice isoform encodes for a 148 aa tetraspan membrane protein. Patient mutations predominate towards the middle, with one prevalent p.R73 change occurring repeatedly. Missense, nonsense and splice mutations were identified. **(d)** Evolutionary conservation of mutated amino acids. **(e)** Patient mutations lead to unstable protein products. Western blot of whole lysate of cells transfected with a cDNA encoding wild type (WT) vs. patient missense mutations, compared with control (p.V71L). Each mutation resulted in the production of 40-50% of WT protein levels, compared with α-tubulin loading control.

Europe PMC Funders Author Manuscripts

Europe PMC Funders Author Manuscripts

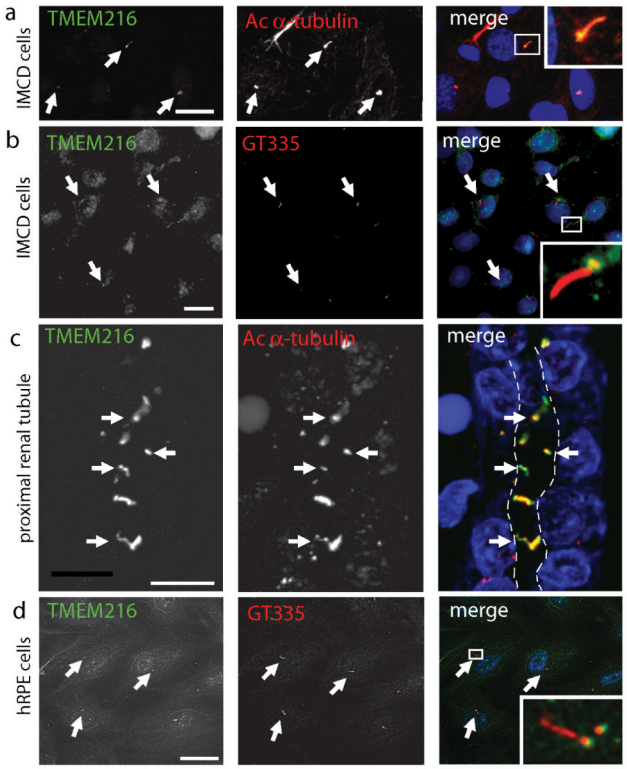

Figure 2.

Ciliary localization of TMEM216. (**a-d**) Overlapping localization of endogenous TMEM216 (green) and acetylated α-tubulin or GT335 (glutamylated tubulin) (red) at the base of the primary cilium (arrows) in IMCD3 (a, b), proximal renal tubules (c) or hRPE cells (d). White dashed line indicates the tubule lumen. Boxes show insets at magnification x10. Scale bar 5 μm.

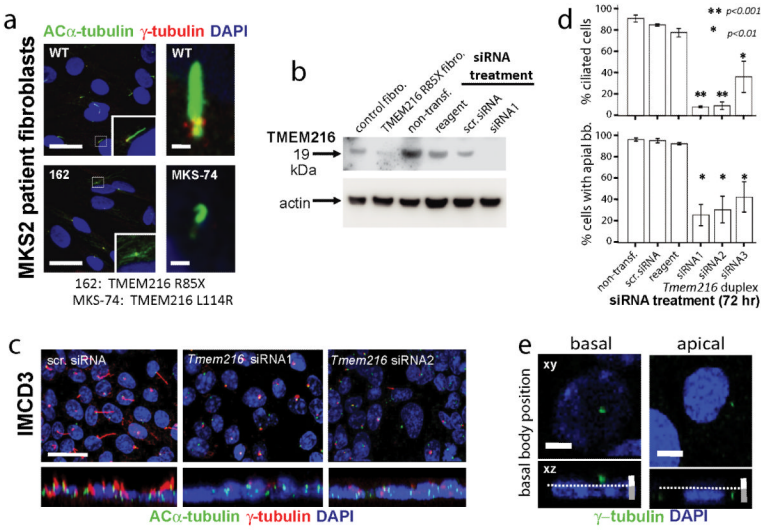

Figure 3.

TMEM216 mutation or knockdown results in impaired ciliogenesis and centrosome docking. **(a)** Two different *TMEM216*-mutated patient fibroblasts lines show defective ciliogenesis and impaired centrosome docking (marked by γ-tubulin). Scale bar: left 20 μm; right 1 μm. **(b)** TMEM216 antisera reacts with a 19 kDa band in control cells, which is reduced in *TMEM216* p.R85X fibroblasts (some residual is apparent likely due to read-through from geneticin treatment), as well as in siRNA1-treated IMCD3 cells. Fibro. = fibroblasts; Non-transf. = non-transfected; scr. = scrambled. **(c)** Transfected IMCD3 cells showing effect of *Tmem216* siRNA treatment, with reduced ciliogenesis and centrosome docking (note lack of cilia and lack of apically located centrosomes following knockdown). Top is *x-y*, and bottom is *x-z* projection, scale bar 10 μm. **(d)** Percent ciliated cells (defined as cilia > 1 μm length) is reduced following *Tmem216* siRNA treatment. Percent cells with apical basal bodies (defined as most superior 1.0 μm sections compared to nuclear position) is similarly reduced. *p<0.01, **p<0.001, chi-squared test. (**e**) Shows method of quantification at 72 hrs. Scale bars: white, most apical 1.0 μm; grey, basal 1.5 μm.

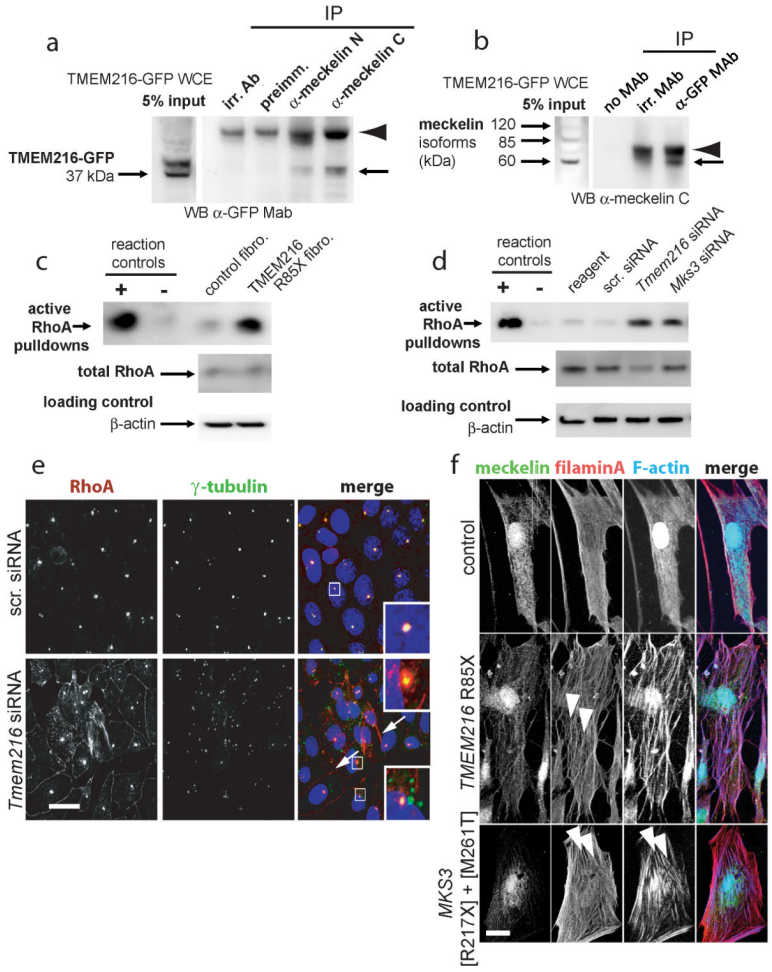

Figure 4.

TMEM216 complexes with Meckelin, and their loss results in Rho hyperactivation and actin cytoskeleton remodelling. **(a)** TMEM216-GFP (~37 kDa; arrow) is immunoprecipitated (IP) with anti-Meckelin antisera against either the N- or C-termini from whole cell extract (input WCE), but not in control IPs with an irrelevant antibody (irr. Ab) or the preimmune antiserum (preimm.). Arrowhead is IgG heavy chain. **(b)** IP of TMEM216-GFP by α-GFP pulls down a 60 kDa C-terminal containing isoform of endogenous Meckelin (arrow), but not in control IPs with no antibody (no MAb) or an irrelevant antibody (irr. MAb). Arrowhead is IgG heavy chain. **(c)** MKS2 fibroblast (fibro.) WCE has increased levels of activated RhoA-GTP compared to normal control. **(d)** siRNA knockdown of *Tmem216* and *Mks3* in IMCD3 cells increased RhoA activation, compared with scrambled control (scr.). Total RhoA and β-actin are loading controls. Positive control (+) is loading with non-hydrolyzable GTPγS, negative control (−) is loading with GDP. **(e)** RhoA (red) localizes to the basal bodies (γ-tubulin, green) in IMCD3 cells following 24 hr treatment with scrambled siRNA, but mislocalizes to regions adjacent to the basal bodies (arrows; and inset, magnification x5) and at basolateral surfaces (arrowheads) following *Tmem216* knockdown. Mislocalization of γ-tubulin is also apparent (bottom inset). Scale bar 10 μm. **(f)** Subcellular phenotypes of fibroblasts cultured from undiseased control and two MKS fetuses mutated in *TMEM216* [p.R85X homozygous] and *MKS3* [p.R217X]+[p.M261T], as indicated. Actin stress fibers in both mutated cells (arrowheads) are detected by phalloidin staining. Scale bar 10 μm.

Europe PMC Funders Author Manuscripts

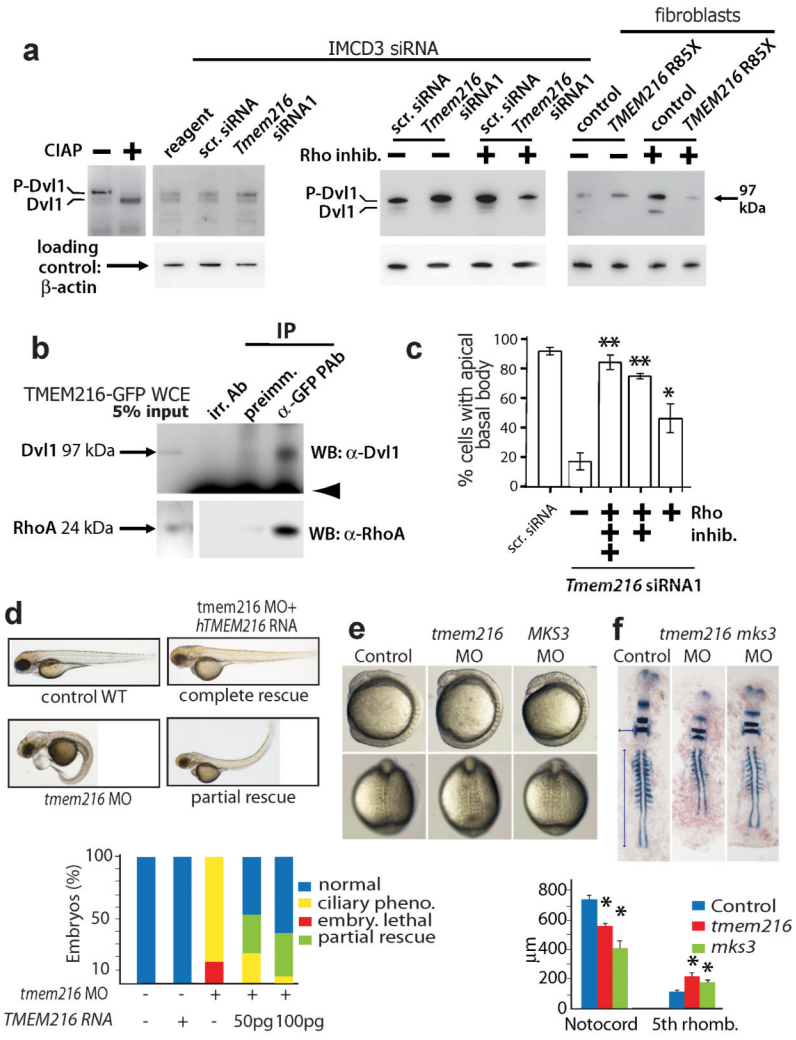

Figure 5.

TMEM216 disruption results in Dvl1 phosphorylation, and planar cell polarity-like phenotypes in zebrafish. **(a)** siRNA knockdown of *Tmem216* (*left panel*) and *TMEM216* p.R85X patient fibroblasts (*right panel*) cause an increase in the upper (phosphorylated) isoform (P-Dvl1) compared to scrambled control (scr.). Treatment with Rho inhibitor exoenzyme-C3-transferase (2 μg/ml) alone increased Dvl1 phosphorylation, but increases in P-Dvl1 by TMEM216 loss are reversed by Rho inhibition (*right panel*). **(b)** Co-immunoprecipitation of both Dvl1 and RhoA with TMEM216 in TMEM216-GFP transfected cells. Arrowhead is IgG heavy chain. **(c)** Dose-dependent rescue of centrosome/basal body docking phenotype in *Tmem216* siRNA-treated cells following += 0.5, ++= 1.0, +++= 2.0 μg/ml Rho inhibitor treatment. *p<0.01; **p<0.001 for chi-squared test. **(d)** Injection of translation-blocking morpholino (MO) to *tmem216* vs. scrambled MO causes a ciliary defect phenotype in injected zebrafish embryos (>50 each condition). Injection of human *TMEM216* RNA causes no phenotype in WT embryos, but allows partial, dose-dependent rescue of the MO phenotype. **(e)** Lateral (top) and dorsal (bottom) views of zebrafish embryos injected with *tmem216* or *mks3* MO at 8-somite stage had ciliopathy features. **(f)** Representative 11-somite stage embryos hybridized with *krox20, pax2,* and *myoD* riboprobes. Convergence to the midline is measured by the width at the fifth rhombomere (horizontal arrow), and extension along the anterior-posterior (AP) axis by

Europe PMC Funders Author Manuscripts

notochord length (vertical arrow) (n=12-15 embryos/injection). Suppression of the *tmem216* or *mks3* morphant gastrulation defect causes significant differences in width and length compared to controls (*p<0.005). Pheno.=phenotype; embry.=embryonic; rhomb.=rhombomere; Bars=standard error of means.

Europe PMC Funders Author Manuscripts

Europe PMC Funders Author Manuscripts

Nat Genet. Author manuscript; available in PMC 2011 January 01.

Table 1

Clinical and molecular data of *TMEM216* mutated families

Family data			Clinical data					Genetic data	
Fam	**Age (sex)**	**Origin**	**CNS**	**Eye**	**Kidney**	**Liver**	**Other**	**Nucleotide changes**	**Protein alterations**
Joubert syndrome related disorders									
COR000	11y, M 15y, F 20y, F 29y, M	Italian	MTS	-	NPH	ELE	-	c.218G>T	p.R73L
	15y, F		MTS	-	NPH	-	-		
	20y, F		MTS	-	NPH	-	-		
	29y, M		MTS	-	NPH	-	-		
COR284	22y, F	Italian	MTS		NPH			c.218G>T	p.R73L
COR114/ F37	1m, M	Turkish	MTS	MicroC	CK	BDP	PD	c.218G>A	p.R73H
	13w, M *		Ec				PD, BLB		
F401		New Zealand	MTS	+	NPH			c.217C>T c.398T>G	p.R73C p.L133X
COR076	1y, F fetus	Ashk	MTS, PMG	-			ToF	c.218G>T	p.R73L
COR287	3m, M	Ashk	MTS				PD	c.218G>T	p.R73L
MTI005	13y, M	Euro	MTS	OMA	NPH?	-	CD	c.218G>T	p.R73L
	3y, F		MTS	OMA		-	CD		
MTI161	4y, M	Ashk	MTS	OMA, Nys	-	-	PD, TT, MP	c.218G>T	p.R73L
MTI214	4y, F	Ashk	MTS	OMA	-	-	CMD	c.218G>;T	p.R73L
MTI467	fetus	Ashk	MTS, DWM		-	-	PD, MOF, CD, HYPT	c.218G>;T	p.R73L
MTI585	1y, F	Ashk	MTS	Co	ACMD	-	CMD	c.218G>;T	p.R73L
MTI658	8y, F	Ashk	MTS	Nys	NPH?	-	PD, CMD	c.218G>;T	p.R73L
	5y, F		MTS	Nys	NPH?	-	PD, CMD		

Europe PMC Funders Author Manuscripts

Family data			Clinical data					Genetic data	
Fam	**Age (sex)**	**Origin**	**CNS**	**Eye**	**Kidney**	**Liver**	**Other**	**Nucleotide changes**	**Protein alterations**
	2 fetuses						PD		
MTI1006	9y, M	Ashk	MTS	OMA, Nys	-	-	-	c.218G>;T	p.R73L
	1y, M (cousin)		MTS	OMA, Nys	-	-	PD		
MTI1008	4y, F	Ashk	MTS, DWM	OMA			RTP	c.218G>;T	p.R73L
Meckel syndrome									
F2	21w, M	Tunisian	Mc		CK	BDP	PD, CP, BLB	c.341T>G	p.L114R
	14w, F		An		CK	BDP	PD, BLB		
F5	24w, M	Tunisian	Mc	MicroO	CK	BDP	PD, CP, IUGR, BLB, HypoG	c.341T>G	p.L114R
F56	fetus	Palestinian	An		CK			c.230G>C	p.G77A→splice: p.T78KfsX30
	15w		DW, Ec		CK		IUGR		
F58	SB, M	Palestinian	Ec		CK	BDP	PD, CP	c.230G>C	p.G77A→splice: p.T78KfsX30
	1day		Ec		CK	BDP	PD		
F154	22w SB	Palestinian	Mc		CK			c.230G>C	p.G77A→splice: p.T78KfsX30
A2423	21w, M	British	Ec		CK	BDP	PD, CP, VSD, IM, BLB	c.253C>T	p.R85X
	12w, M		Ec		CK	-	CH, Omph		

Legend: -: not affected; ACMD: abnormal cortico-medullary differentiation; An: anencephaly; Ashk: Ashkenazi Jewish; BDP: bile ducts proliferation; BLB: bowing of long bones; CD: clinodactyly; CH: cystic hygroma; CK: cystic kidneys; CMD: camptodactyly; Co: chorioretinal coloboma; CP: cleft palate; CVA: cerebellar vermis agenesis; DW: Dandy-Walker malformation; Ec: encephalocele; ELE: elevated liver enzymes; Euro: European; F: female; HypoG: hypoplastic external genitalia; HYPT: hypertelorism; IM: intestinal malrotation; IUGR: intrauterine growth retardation; M: male; m: months; IUGR: intrauterine growth retardation; Mc: meningocele; MEc: meningoencephalocele; MOF: multiple oral frenulae; MicroC: microcornea; MicroO: microphthalmia; MP: micropenis; MTS: molar tooth sign; NPH: nephronophthisis; Nys: nystagmus; OMA: oculomotor apraxia; Omph: omphalocele; PD: polydactyly; PMG: polymicrogyria; RTP: rhythmic tongue protrusions; SB: stillbirth; ToF: tetralogy of Fallot; TT: tongue tumors; VSD: ventricular septal defect; w: gestational weeks; y: years. Empty cells denote unavailable clinical information;

*MKS fetus.